ELSEVIER

Chemical Engineering Journal 131 (2007) 301–317

Chemical Engineering Journal

www.elsevier.com/locate/cej

Analysis of environmental benefits of CFB combustors via one-dimensional model

A. Gungor *, N. Eskin

Istanbul Technical University, Mechanical Engineering Faculty, Gumussuyu 34437, Istanbul, Turkey

Received 15 March 2006; received in revised form 2 November 2006; accepted 7 December 2006

Abstract

Superior environmental performance of CFB combustors is one of the prime motivations of its extensive use in industry. A well-designed CFB combustor can burn coal with high efficiency and within acceptable level of emission pollutants. The carbon monoxide, carbon dioxide, sulphur dioxide, nitrogen oxide and char content in stack gases are the major emission pollutants in CFB combustors with respect to atmospheric environmental conditions. This paper presents a modeling study of environmental pollutions resulting from coal combustion in a CFB combustor. Using this model, the variations of these emissions along the combustor height with different operational conditions such as particle diameter, bed operational velocity and excess air are investigated. The simulation results are compared with test results obtained from the 50 kW Gazi University Heat Power Laboratory pilot scale unit and good agreement is observed. The present study proves that CFB combustion allows clean and efficient combustion of coal which is demonstrated by the fact that both experimental data and model simulation results have low and acceptable level of emission pollutants.

Keywords: Circulating fluidized bed; Modeling; Environmental pollutions; NO emissions; SO_2 emission

1. Introduction

As the combustion of fossil fuels today is the most important cause of environmental problems, circulating fluidized bed (CFB) combustors are environmental friendly applications, which can be directly reflected in better combustion conditions. CFB combustors have the ability to burn a wide variety of solid fuels with low pollutant emissions, high combustion efficiency, having smaller combustor cross section, fewer feed points, good turndown and load capability. Operating either in the fast fluidization regime or in the transported bed regime, CFB combustors have many advantages over the conventional bubbling or turbulent fluidized bed combustors, such as high gas–solids contact efficiency, high gas and solids throughput, reduced axial dispersion of both gas and solids phases, and so on.

Because of containing complex gas–solid flow and gas-phase reactions, modeling of CFB combustors is rather difficult. The fluid dynamics of this gas–solid two-phase flow is very complex and strongly dominated by particle to particle interactions. Furthermore, the numerous homogeneous and heterogeneous catalytic gas-phase reactions and their kinetics for the description of the combustion phenomena and the emission formation and destruction are not completely known. The main goal of the modeling of CFB combustors is to constitute a system that maximizes combustion efficiency, and minimizes operating and investment costs and air pollutant emissions. It is also important to determine the effects of operational parameters in CFB combustors via simulation study instead of expensive and time-consuming experimental studies.

The coal combustion modeling has been dealt with in a number of efforts by either 1D, 1.5D, 2D or 3D approaches. Basu [1] presented a comprehensive review of combustion of coal in CFBs. In that study, coal combustion models can be grouped under three levels of details of sophistication. *Level I*—the simplest model is 1D with plug flow reactor, where solids are back-mixed [2–4]. The 1D models do not consider the solid flow in the annular region of the riser, where temperature, gas concentration and velocity can differ from that in the core, in which an up-flowing dilute region is considered. *Level II*—core-annulus, 1.5D, with broad consideration of combustion and other related processes [5–9]. *Level III*—3D model based on Navier Stokes equation [10–12].

* Corresponding author. Tel.: +90 505 504 49 02; fax: +90 212 245 07 95.
E-mail address: afsingungor@hotmail.com (A. Gungor).

1385-8947/$ – see front matter © 2006 Elsevier B.V. All rights reserved.
doi:10.1016/j.cej.2006.12.012

Nomenclature

A_{ca}	interfacial area between core and annulus (m^2)
Ar	Archimedes number
$c_{p,g}$	heat capacity of gas (kJ/kmole K)
$c_{p,s}$	heat capacity of solids (kJ/kg K)
C	gas concentration (kmole/m^3)
d_p	particle diameter (m)
D	bed diameter (m)
D_b	equivalent bubble diameter (m)
D_g	diffusivity coefficient for oxygen in nitrogen (m^2/s)
EA	excess air
f_w	solid mixing parameter, ratio of wake volume to the bubble volume including the wakes
G_{ca}	solid flux from core to annulus (kg/m^2s)
h_i	height above the distributor (m)
H	enthalpy (kJ/kg)
H_b	combustor height (m)
k	rate constant (m/s)
k_a	attrition constant
k_{be}	mass transfer coefficient (s^{-1})
k_c	char combustion reaction rate (kg/s)
k_{ca}	solid dispersion constant from core to annulus (m/s)
k_{cr}	kinetic rate (s^{-1})
k_{cd}	diffusion rate (s^{-1})
k_g	gas conduction heat transfer coefficient (W/m K)
k_L	reaction rate (s^{-1})
k_{vL}	volumetric reaction rate (kg/m^2s)
m	mass in cell (kg)
$\Delta\dot{m}_C$	carbon mass flow rate consumed from physical/chemical process (kg/s)
m_{col}	total solid particle holdup (kg)
$\dot{m}$	mass flow rate (kg/s)
$\dot{m}_{char,burn}$	burnt char mass flow rate (kg/s)
M	molecular weight (kg/mole)
$\dot{n}$	gas flow rate (kmole/s)
$\Delta\dot{n}$	gas flow rate consumed from chemical processes (kmole/s)
P	pressure (Pa)
PA/SA	Primary to secondary air ratio
q	isokinetic gas volume (m^3)
$\dot{Q}$	amount of heat transferred (kW)
r	reaction rate (mole/s, mole/cm^3s)
r_i	radius of the coal particle (m)
R_a	particle attrition rate (kg/s)
R_c	radius of the core region (m)
Re	Reynolds number
R_g	gas constant (kJ/mole K)
R_u	Universal gas constant (kJ/mole K)
S_g	specific surface area (m^2/kg)
Sc	Schmidt number
Sh	Sherwood number
T	bed temperature (K)
T_{core}	temperature of the core region (K)
T_{ann}	temperature of the annulus region (K)
U_{mf}	minimum fluidization velocity (m/s)
U_t	particle terminal velocity (m/s)
U_0	superficial velocity (m/s)
ΔV	volume of the cell (m^3)
W_b	mass of particle (kg)
X_c	weight fraction of the carbon in the coal (kg-carbon/kg-coal)
X_k	char mass fraction (kg-char/kg-bed material)
y	mass fraction of gas species (kg-gas species/kg-gas)

Greek letters

δ	thickness of the annulus (m)
ε	void fraction
ε_b	bubble volume fraction
λ_s	reactivity of limestone
μ	gas viscosity (kg/ms)
ρ	particle density (kg/m^3)
Φ	mechanism factor

Subscripts

ann	annulus
ash	ash
b	bubble
burn	burn
c	core
cell	cell
core	core
C	carbon
e	emission
g	gas
mf	minimum fluidization
p	particle
s	solid
wall	wall

Nitrogen oxides are a major environmental pollutant resulting from combustion. The reactions of nitric oxide with carbons or chars are of current interest with regard to their possible role in reducing NO emissions from combustion systems. They also offer new useful insights into the oxidation reactions of carbons, generally [13]. A large literature concerning these reactions has developed, as evidenced in three reviews [14–16] and by the recent publication of many papers in the area [17–25]. These works have suggested considerable complexity in the mechanisms of NO reduction and a large variability in reported kinetics. There are two approaches to describe NO_x emission in CFB [22]. The first approach involves overall reaction (15 reactions considering catalytic activity of CaO and char). The overall rate constants are measured preferably under CFB conditions [23]. The other approach is more thorough, and is based on actual chemical reactions whose rate constants can be taken from literature [24]. For CFB only 106 reactions with 28 species were used to model the NO_x emission. However, a detailed review

shows that all N-related reactions have not the same importance [25]. So instead of considering all N-related reactions, one could use only the important reactions for the development of a predictive procedure for the overall NO emission from a CFB combustor.

Circulating fluidized bed coal combustion with sorbent addition allows clean combustion of coals of different rank even with high sulphur and ash contents. Numerous experimental and theoretical studies about the sulphur retention in CFB combustors are present in the literature [18,26–28]. Some models have already been proposed for predicting the sulphur retention in CFB combustor, but there are important differences between their sub-models, especially as far as the CFB hydrodynamics is considered [18,26–28].

Because coal combustion in a CFB combustor directly is affected by its hydrodynamic parameters, both hydrodynamic and combustion models are treated simultaneously to yield a predictive model for the CFB combustor. It has been widely accepted that a CFB combustor may be characterized by two flow regimes: a dense bed at the bottom and a dilute region above the secondary air inlet. There are great differences in the hydrodynamics between the dense bed and the dilute region. However, most of the models in the literature do not completely take account of the performance of the dense bed, consider the dense bed as well-mixed distributed flow with constant voidage, and use generally lumped formulation [1–4,6–9,10–28]. Experimental evidence has been reported by Svensson et al. [29], and Werther and Wein [30] that, the fluid-dynamical behavior of the dense bed is similar to that of bubbling fluidized beds. The results of studies of Leckner et al. [31] and Montat et al. [32] imply that the combustion of coal, particles mixing and heat transfer in the dense bed dominate the performances of CFB. This implies that, dense bed should be modeled in detail as two-phase flow. Therefore in this study, dense bed is modeled as two-phase flow which constitutes a major difference from the previous studies in the literature.

The objective of the present work is to develop a 1D model which simultaneously treats hydrodynamic and coal combustion models in order to allow a detailed examination of how each operational parameter might influence the environmental pollutions resulting from coal combustion.

In the modeling, the CFB riser is analyzed in two regions. The bottom zone (dense bed) is considered as a bubbling fluidized bed in turbulent fluidization regime and is modeled in detail as two-phase flow. The flow domain is subdivided into a solid-rare bubble phase and a solid-laden emulsion phase. The upper zone (dilute region) is considered as core-annulus flow structure.

Developed model includes devolatilization, attrition and combustion of a char particle, respectively which also simultaneously predicts the carbon concentration, O_2, CO, CO_2, NO, SO_2, V.M. (volatile matter) distributions, particle size distribution, solid mass flux, and bed temperature values along the bed height. Another advantage is that the model takes into account the NO and SO_2 reduction which are major environmental pollutants. The model which simultaneously predicts both hydrodynamic and combustion aspects has been validated against the data from the literature [33]. Additionally, this model investigates effects of different operational parameters (particle diameter, bed operational velocity and excess air) on environmental pollutions.

2. Modeling

Designing of the CFB combustor is very important because of burning coal with high efficiency and within acceptable levels of gaseous emissions. A very good appreciation of the combustion and pollutant generating processes is needed for a reliable performance prediction through modeling and can greatly avoid costly upsets. The present CFB combustor model can be divided into three major parts: a sub-model of the gas–solid flow structure; a reaction kinetic model for local combustion and a convection/dispersion model with reaction. The latter formulates the mass balances for the gaseous species and the char at each control volume in the flow domain. Kinetic information for the reactions is supplied by the reaction kinetic sub-model, which contains description of devolatilization and char combustion, and emission formation and destruction, respectively.

2.1. Hydrodynamics structure

Hydrodynamics plays a crucial role in defining the performance of CFBs. Combustor hydrodynamic is modeled taking into account previous work [34].

The flow structure of CFBs is known to exhibit axial nonuniformities [35]. In order to characterize this behavior, the riser is subdivided vertically into zones with different properties. According to the axial solid volume concentration profile, the riser is axially divided into two different zones: the bottom zone and the upper zone.

2.1.1. Bottom zone (dense bed)

As mentioned above, most of the models in the literature do not completely take account of the performance of the dense bed, consider the dense bed as well-mixed distributed flow with constant voidage, and use generally lumped formulation [1–4,6–9,10–28]. In this study, the bottom zone is considered as a bubbling fluidized bed in turbulent fluidization regime and is modeled in detail as two-phase flow.

In the literature, both Leckner et al. [31] and Huilin et al. [36] claim that this zone could be explained by the presence of bubble-like voids that characterizes the gas flow. Werther and Wein [30] described the expansion behavior of the turbulent CFB bottom zone by a model that is based on modified equations which were originally developed for conventional bubbling fluidized beds. These results lead to the conclusion that in the bottom zone of CFB reactors another two-phase flow structure is established with a solid-rare bubble phase and a solid-laden emulsion phase. In the model, the flow domain is subdivided into *n* control volumes that each one has a solid-rare bubble phase and a solid-laden emulsion phase. The bubble rise velocity, the bubble size, the bubble volume fraction and the suspension porosity is calculated by extrapolating the Eskin and Kılıç [37] bubbling-bed model which has been validated against the experimental data as given in previous work [38] to the high gas velocities

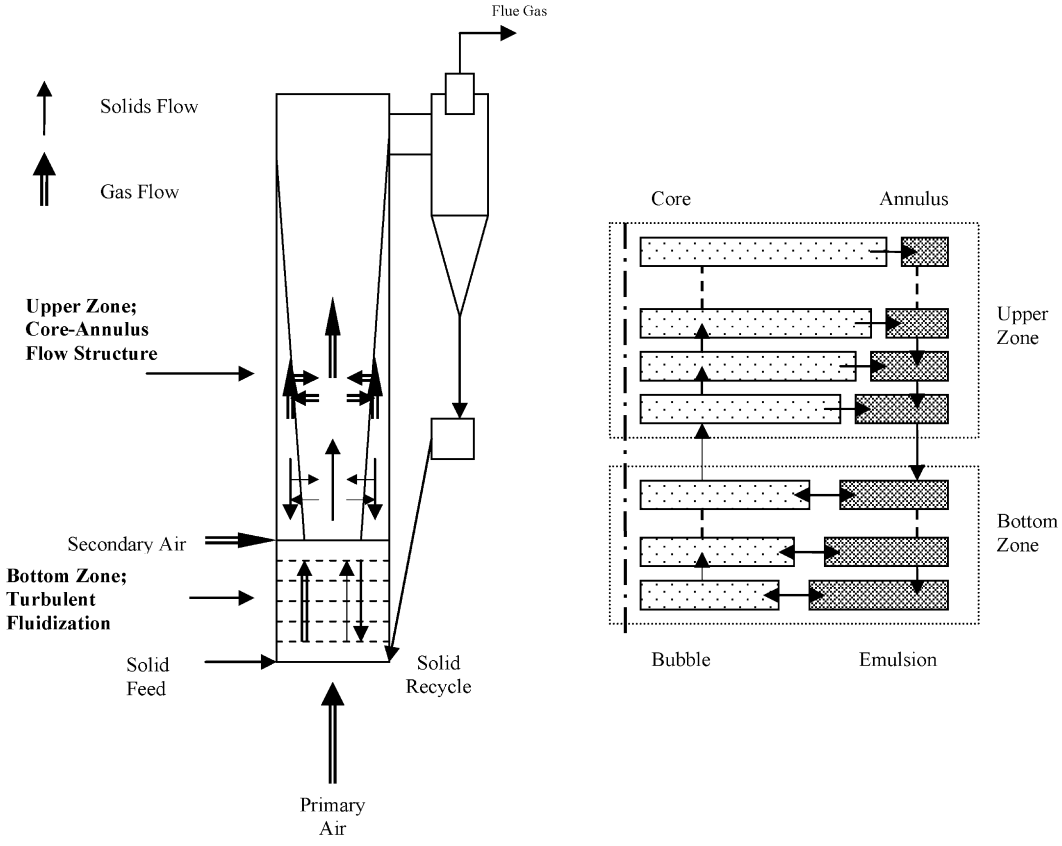

Fig. 1. The scheme of the CFB combustor.

used in the CFB. Fig. 1 shows a schematic diagram of the system considered.

In CFB combustors, there is an internal material circulation within the combustor. As the gases move upward in the combustor, particles are transported upwards with the gas flow in the bubble phase and in the core region. The particles are falling downwards, because the gas velocity is lower near to the walls in the annulus region and in the emulsion phase and form internal material circulation inside the combustor. In this study in the bottom zone, this material circulation is modeled through the single-phase back-flow cell model as shown in Fig. 2.

The overall material balance for the solids in the ith control volume, in terms of the backmix flow in emulsion and bubble phases, $\dot{m}_{e,i}$ and $\dot{m}_{b,i}$ is given by the following equation.

$$\left(\frac{dm}{dt}\right)_i = \dot{m}_{b,i-1} - \dot{m}_{b,i} + \dot{m}_{e,i+1} - \dot{m}_{e,i} - \dot{m}_{burn,i} + \dot{m}_{ash,i} \quad (1)$$

The material balance for the carbon in the ith control volume is given as follows:

$$\left(\frac{d(mX_c)}{dt}\right)_i = \dot{m}_{b,i-1}X_{c,i-1} - \dot{m}_{b,i}X_{c,i} + \dot{m}_{e,i+1}X_{c,i+1} - \dot{m}_{e,i}X_{c,i} - \dot{m}_{char,burn,i} \quad (2)$$

where $X_{c,i}$ is the weight fraction of carbon and $\dot{m}_{char,burn,i}$ is char mass flow rate burnt in the control volume.

A two-phase model is used for gas phase material balance. The material balances are made for gases, O_2, CO, CO_2, SO_2, NO, and for water vapor in the bubble and emulsion phases. The material balance for the gas phase in the ith control volume for emulsion and bubble phases, are given below, respectively.

$$\left(\frac{dn_k}{dt}\right)_{e,i} = \dot{n}_{e,k,i-1} - \dot{n}_{e,k,i} - k_{be}\Delta V_i \varepsilon_{b,i}(C_{e,k,i} - C_{b,k,i}) + \Delta\dot{n}_{e,k,i} \quad (3)$$

$$\left(\frac{dn_k}{dt}\right)_{b,i} = \dot{n}_{b,k,i-1} - \dot{n}_{b,k,i} + k_{be}\Delta V_i \varepsilon_{b,i}(C_{e,k,i} - C_{b,k,i}) + \Delta\dot{n}_{b,k,i} \quad (4)$$

where $\dot{n}_k$ indicates the gas flow rate of gas components (volatile gases, O_2, CO, CO_2, SO_2, NO, and water vapor in the emulsion phase and O_2, CO_2, SO_2, and NO in the bubble phase, respectively), V_i is the volume of the ith cell (control volume). Gas exchange, between the bubble and the emulsion phases is a function of the bubble diameter and varies along the axis of the riser and it is considered in the model as follows [39];

$$k_{be,g} = \frac{11}{D_b} \quad (5)$$

where D_b is the bubble diameter predicted by a correlation established by Mori and Wen [40].

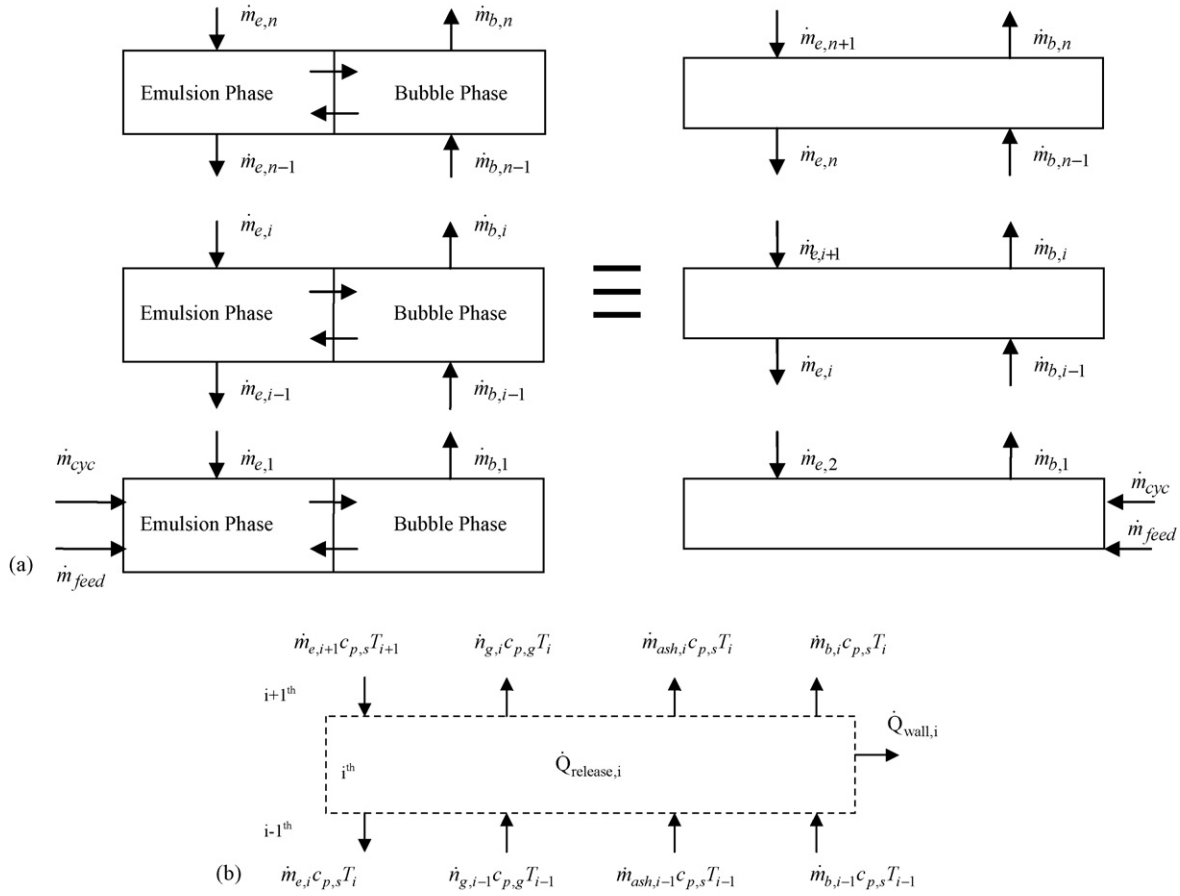

Fig. 2. (a) A single-phase back-flow cell model. (b) The energy balance of the *i*th control volume in the bottom zone.

In the model, the minimum fluidization velocity is obtained according to Wen and Yu [41]:

$$U_{\mathrm{mf}} = \frac{\mu}{Cd_{\mathrm{p}}}[(33.7^2 + 0.0651\mathrm{Ar})^{0.8} - 33.7] \tag{6}$$

where C is the gas mixture concentration in the control volume, d_{p} is the particle diameter, Ar is the Archimedes number. Minimum fluidization voidage ($\varepsilon_{\mathrm{mf}}$) is taken as 0.5 in the model calculations [38]. For the char at the bottom zone, complete vertical mixing is assumed. Char is entering the bottom bed with feed coal, but also from the solid return leg with the recycled solids from the cyclone. The amount of and temperature of recycled solids from the cyclone are taken from experimental data. For simulations with different rates, the cyclone efficiency of the pilot plant is utilized [33].

2.1.2. Upper zone (dilute region)

For the upper zone, core-annulus flow structure with a net dispersion of solids from the core to the annulus is used. Within the core and the annulus, there are no radial suspension density gradients, while the lateral dispersion between the core and the annulus is considered. It is also assumed that the char is flowing up and downwards with the same velocity as the bed material in the core and in the annulus, respectively. Thickness of the annulus, δ, varies according to the bed height and it is calculated as follows [30],

$$\frac{\delta}{D} = 0.55Re - 0.22\left(\frac{H_{\mathrm{b}}}{D}\right)^{0.21}\left(\frac{H_{\mathrm{b}} - h_i}{H_{\mathrm{b}}}\right)^{0.73} \tag{7}$$

where H_{b} is the combustor height, h_i the height above the distributor and D is the bed diameter. The overall material balance for the solids in the *i*th control volume, in the core and in the annulus regions is given as follows, respectively.

$$\left(\frac{\mathrm{d}m}{\mathrm{d}t}\right)_{\mathrm{core},i} = \dot{m}_{\mathrm{core},i-1} - \dot{m}_{\mathrm{core},i} - A_{\mathrm{ca},i}G_{\mathrm{ca},i} - \dot{m}_{\mathrm{burn,core},i} + \dot{m}_{\mathrm{ash,core},i} \tag{8}$$

$$\left(\frac{\mathrm{d}m}{\mathrm{d}t}\right)_{\mathrm{ann},i} = \dot{m}_{\mathrm{ann},i+1} - \dot{m}_{\mathrm{ann},i} + A_{\mathrm{ca},i}G_{\mathrm{ca},i} - \dot{m}_{\mathrm{burn,ann},i} + \dot{m}_{\mathrm{ash,ann},i} \tag{9}$$

where G_{ca} is the solid flux from core to annulus and is obtained according to Hua et al. [8].

$$\frac{\mathrm{d}G_{\mathrm{ca}}}{\mathrm{d}z} = -\frac{2\rho k_{\mathrm{ca}}[(1-\varepsilon_{\mathrm{c}}) - (1-\varepsilon)]}{R_{\mathrm{c}}} \tag{10}$$

where R_{c} is the radius of the core region ($R_{\mathrm{c}} = D/2 - \delta$), and k_{ca} is the solid dispersion coefficient from core to annulus. To calculate the flow rate of solids rising through the core and descending

through the annulus, the Rhodes model was used [8]. In this model the flow rate of solids transferred from the core to the annulus is proportional to the solids concentration present in the core and to the interface surface. The solids dispersion constant was calculated using the following equation, determined experimentally:

$$k_{ca} = \frac{0.14}{U_0 - U_t} \tag{11}$$

where U_0 is the superficial velocity and U_t is the particle terminal velocity. The material balance for the gas phase in the ith control volume for core and annulus regions are given as follows, respectively.

$$\left(\frac{dn_k}{dt}\right)_{core,i} = \dot{n}_{core,k,i-1} - \dot{n}_{core,k,i} - k_{ca}A_{ca,i}(C_{core,k,i}\varepsilon_{core,i} - C_{ann,k,i}\varepsilon_{ann,i}) + \Delta\dot{n}_{core,k,i} \tag{12}$$

$$\left(\frac{dn_k}{dt}\right)_{ann,i} = \dot{n}_{ann,k,i-1} - \dot{n}_{ann,k,i} + k_{ca}A_{ca,i}(C_{core,k,i}\varepsilon_{core,i} - C_{ann,k,i}\varepsilon_{ann,i}) + \Delta\dot{n}_{ann,k,i} \tag{13}$$

where $\dot{n}_k$ indicates the gas flow rate of gas components (O_2, CO, CO_2, SO_2, and NO in the core region and volatile gases, O_2, CO, CO_2, SO_2, NO, and for water vapor in the annulus region, respectively). Gas exchange between core and annulus is assumed to be the same with the solid dispersion coefficient in the model.

2.1.3. Attrition

The solids inventory in a CFB combustor consists of spent and reacting fuel and sorbent particles and inert bed materials. Char is entering the bottom zone with the feed coal but also from the solid return leg with the recycled solids from the cyclone. The particle size distribution of coal particles depend on attrition and combustion in the model. The Sauter mean diameter is adopted as average particle size. In the fluidized beds, particle attrition takes place by surface abrasion, i.e., particles of a much smaller break away from the original particle. The upper limit size of the fines produced is in the range 50–100 μm [35,42]. The attrition rate is influenced by many factors including particle properties, solids concentration, particle size, residence time and superficial gas velocity. However, particle properties and gas velocity may have more great influences [43–45]. In the model, the attrition rate is assumed to be the same as for the bottom zone and the upper zone and is calculated as follows [7,8,42];

$$R_a = k_a(U_0 - U_{mf})\frac{W_b}{d_p} \tag{14}$$

where W_b is the mass of particle, U_{mf} is the minimum fluidization velocity and k_a is the attrition constant and is obtained varying in the range (2–7) $\times 10^{-7}$ with a superficial gas velocity of 4–6 m/s and a circulating solids mass flux from 100 to 200 kg/m^{2}s [7]. In the model, the attrition constant value is taken as 2×10^{-7} for Tuncbilek lignite [46]. In this work, it is assumed that the particle size of limestone particles does not change during reaction; the attrition of limestone particles is not considered.

2.2. Kinetic model

The char comprises mainly carbon, ash, nitrogen and sulphur. Combustion of coal is depending on oxygen presence in the bed. Above 750 °C, char oxidizes to gaseous products; CO, CO_2, SO_2 and NO. The combustor model takes into account, the devolatilization of coal, subsequent combustion of volatiles followed by residual char.

A large part of the chemical energy in coal is released through devolatilization. The combustion rate of char, which is left after devolatilization, is an order of magnitude less than the devolatilization rate [48]. The degree of devolatilization and its rate increase with increasing temperature [49]. However, a more detailed work of Stenseng et al. [23] shows that volatiles may continue to burn in the upper zone under certain conditions.

In the model, volatiles are entering the combustor with the fed coal particles. It is assumed that the volatiles are released in emulsion phase in the bottom zone of the CFB combustor at a rate proportional to the solid mixing rate. The volatiles are assumed to be released in two ways. A portion of volatiles proportional of f_w, the solid mixing coefficient (also the fraction of bubble volume occupied by the wake), is released uniformly throughout the bed. The remaining portion of volatiles proportional to $(1 - f_w)$ is released near the coal feed point.

Volatile yield is estimated by the empirical correlations of Gregory and Littlejohn [50] in the model. The composition of the products of devolatilization in weight fractions is estimated from the correlations of Loison and Chauvin [51]. The amount of nitrogen and sulphur increases as a function of bed temperature and is estimated according to the study of Fine et al. [52]. The sulphur and the nitrogen in the residual char are released as sulphur dioxide and NO during the combustion of the char.

The char particles resulting from the devolatilization process consist of the remaining carbon fraction $(1 - X_c)$ and ash only. These particles are then burned to produce a mixture of CO and CO_2 according to the reaction is given in Table 1. The size of char reduces due to combustion as well as due to attrition. Coal particles' behavior during the gas–solid reaction is assumed to be described in terms of shrinking core with attiring shell, i.e., the dual shrinking-core model. Therefore, the changes in particle diameter are taken into consideration in the model. The rate at which particles of size r_i shrink as follows [8,47]:

$$r(r_i) = -\frac{dr_i}{dr} = \frac{12C_{O_2}}{\rho X_k(1/k_c + d_p/Sh D_g)} \tag{15}$$

where C_{O_2} is the oxygen concentration around the particle, D_g the diffusion coefficient for oxygen, X_k is the char weight fraction, k_c is the char combustion reaction rate and Sh is Sherwood number. After the combustion of char, ash is the residual product, which takes no part in the combustion reaction. Table 1 shows the reactions and reaction rates used in the model.

Table 1
Reactions and reaction rates using in the model

Reaction	Reaction rate		
$C + \frac{1}{\phi}O_2 \rightarrow \left(2 - \frac{2}{\phi}\right)CO + \left(\frac{2}{\phi} - 1\right)CO_2$	$r_c\ (\text{mol/s}) = \pi d_c^2 k_c C_{O_2}$	$k_c\ (\text{kg/s}) = \frac{R_u T/M_c}{1/k_{cr}+1/k_{cd}}$	$k_{cr}\ (\text{kg/(m}^2\,\text{s kPa)}) = 8710 \exp\left(\frac{-1.4947\times10^8}{R_u T}\right)$ [58] $k_{cd}\ (\text{kg/(m}^2\,\text{s kPa)}) = \frac{12\,Sh\Phi D_g}{d_p R_g T}$ $Sh = \frac{k_g d_p}{D_g} = 2\varepsilon + 0.69\left(\frac{Rep}{\varepsilon}\right)^{1/2} Sc^{1/3}$ [6,8]
$CO + \frac{1}{2}O_2 \rightarrow CO_2$	$r_{CO}\ (\text{mol/cm}^3\,\text{s}) = 3\times10^{10} \exp\left(\frac{-6.699\times10^7}{R_u T}\right) y_{CO} y_{H_2O}^{0.5} \frac{17.5 y_{O_2}}{1+24 y_{O_2}} \left(\frac{P}{R_u T}\right)^{1.8}$ [54]		
$NO + \frac{1}{2}C \rightarrow \frac{1}{2}N_2 + \frac{1}{2}CO_2$	$r_N\ (\text{mol/s}) = \pi d_c^2 k_N C_{NO}$		$k_N\ (\text{m/s}) = 1.3\times10^5 \exp\left(\frac{-17111}{T}\right)$ [19]
$CaO + SO_2 + \frac{1}{2}O_2 \rightarrow CaSO_4$	$k_L\ (\text{s}^{-1}) = \frac{\pi}{6} d_s^3 k_{vL} C_{SO_2}$ [6]		$k_{vL}\ (\text{kg/m}^2\,\text{s}) = 490 \exp\left(\frac{-17,500}{R_g T}\right) S_g \lambda_s$ [55] $S_g = -384 T_g + 5.6\times10^4 \quad T_g \geq 1253\ \text{K}$ $S_g = 35.9 T_g - 3.67\times10^4 \quad T_g < 1253\ \text{K}$

2.2.1. Pollutants released during combustion

As the combustion of fossil fuels today is the most important cause of environmental problems, CFB combustors are environmental friendly applications which can be directly reflected in better combustion conditions. CFB combustors have the ability to burn a wide variety of solid fuels with low pollutant emissions. Sulphur dioxide and nitric oxide are two major air pollutants released from a fossil fuel fired combustor.

2.2.1.1. Sulphur oxides. Circulating fluidized bed coal combustion with sorbent addition allows clean combustion of coals of different rank even with high sulphur and ash contents. During the combustion of coal, the sulphur in it is oxidized to the pollutant, SO_2. Limestone ($CaCO_3$) of the bed materials calcine to CaO which reacts with SO_2 producing $CaSO_4$. Thus, instead of leaving the combustor as a gaseous pollutant, sulphur is discharged as a solid residue. As mentioned above, numerous experimental and theoretical studies about the sulphur retention in CFB combustors are present in the literature [18,26–28]. Some models have already been proposed for predicting the sulphur retention in CFB combustor, but there are important differences between their sub-models, especially as far as the CFB hydrodynamics is considered [18,26–28]. In the model, different SO_2 generation rates, depending on the height in the bed, were considered. These differences were due to differences in the char combustion rate because of the existence of axial oxygen concentration profiles. In CFB combustor the SO_2 generation and retention processes take place simultaneously in the bed. The sulphur retention depends on many factors as gas velocity, Ca/S molar ratio, sorbent particle properties, bed height, solid inventory, etc. Forming calcium sulphate and the reaction rate of a limestone particle considering in the model are given in Table 1.

2.2.1.2. Nitric oxides. Nitrogen oxides are a major environmental pollutant resulting from combustion. The reactions of nitric oxide with carbons or chars are of current interest with regard to their possible role in reducing NO emissions from combustion systems. As mentioned above, large literature concerning these reactions has developed, as evidenced in three reviews [14–16] and by the recent publication of many papers in the area [17–25]. These works have suggested considerable complexity in the mechanisms of NO reduction and a large variability in reported kinetics.

In the model, nitric oxide is produced from the oxidation of both volatile-bound nitrogen and char-bound nitrogen. The production of NO from char-bound nitrogen is proportional to the combustion rate of char [39]. The production of NO from volatile-bound nitrogen is present in the literature [56]. A general guide to the reaction path of NO formation is shown by Amand [48]. NO emissions are reduced by the char in the model according to the reaction given in Table 1.

2.3. The energy equations

In the bottom zone, the overall energy balance equation in the *i*th control volume can be expressed in terms of rate of change

of energy as (Fig. 2):

$$\left(\frac{dE}{dt}\right)_i = \dot{m}_{b,i-1}c_{p,s}T_{i-1} - \dot{m}_{b,i}c_{p,s}T_i + \dot{m}_{e,i+1}c_{p,s}T_{i+1} - \dot{m}_{e,i}c_{p,s}T_i + \dot{m}_{ash,i-1}c_{p,s}T_{i-1} - \dot{m}_{ash,i}c_{p,s}T_i + \dot{n}_{g,i-1}c_{p,g}T_{i-1} - \dot{n}_{g,i}c_{p,g}T_i + \dot{Q}_{release,i} - \dot{Q}_{wall,i} \quad (16)$$

In the upper zone, the overall energy balance equation in the ith control volume can be expressed in terms of rate of change of energy for the core and the annulus regions respectively as:

$$\left(\frac{dE}{dt}\right)_{core,i} = \dot{m}_{core,i-1}c_{p,s}T_{core,i-1} - \dot{m}_{core,i}c_{p,s}T_{core,i} - A_{ca,i}G_{ca,i}c_{p,s}(T_{core,i} - T_{ann,i}) + \dot{m}_{ash,core,i-1}c_{p,s}T_{core,i-1} - \dot{m}_{ash,core,i}c_{p,s}T_{core,i} + \dot{Q}_{release,i} + \dot{n}_{g,core,i-1}c_{p,g}T_{core,i-1} - \dot{n}_{g,core,i}c_{p,g}T_{core,i} - k_{ca}A_{ca,i}c_{p,g}(C_{core,i}\varepsilon_{core,i}T_{core,i} - C_{ann,i}\varepsilon_{ann,i}T_{ann,i}) \quad (17)$$

$$\left(\frac{dE}{dt}\right)_{ann,i} = \dot{m}_{core,i-1}c_{p,s}T_{core,i-1} - \dot{m}_{core,i}c_{p,s}T_{core,i} + A_{ca,i}G_{ca,i}c_{p,s}(T_{core,i} - T_{ann,i}) + \dot{m}_{ash,core,i-1}c_{p,s}T_{core,i-1} - \dot{m}_{ash,core,i}c_{p,s}T_{core,i} + \dot{Q}_{release,i} - \dot{Q}_{wall,i} + \dot{n}_{g,core,i-1}c_{p,g}T_{core,i-1} - \dot{n}_{g,core,i}c_{p,g}T_{core,i} - k_{ca}A_{ca,i}c_{p,g}(C_{core,i}\varepsilon_{core,i}T_{core,i} - C_{ann,i}\varepsilon_{ann,i}T_{ann,i}) \quad (18)$$

where $\dot{Q}_{released,i}$, the amount of heat released from combustion of coal [53], carbon monoxide [54] and volatiles [54,57], and $\dot{Q}_{wall,i}$ the amount of heat transferred to the wall.

3. Numerical solution

The CFB combustor is divided into cells treated as control volumes along gas and solid flow path for solving the model. These cells are homogenous, fully mixed sections. Each cell in the bottom zone is divided into two parts: a solid-rare bubble phase and a solid-laden emulsion phase at the bottom zone. A single-phase back-flow cell model is used to represent the solid mixing in the bottom zone. Each cell in the upper zone is divided into two parts: core and annulus, and each part treated as one balance section. The simulated results are obtained by using a combined Relaxation Newton–Raphson method with a computer code developed by the authors in FORTRAN language. Flow chart of the numerical solution of the model is shown in Fig. 3.

4. Results and discussion

In order to verify the validity of the developed model, simulation results are compared with the experimental data obtained from 50 kW pilot CFB combustor using lignite [33]. The overall dimensions are 1.80 m in height and it has a circular cross-section with a diameter of 0.125 m as shown in Fig. 4. A more detailed description of the experimental apparatus is given elsewhere [58]. The combustion air is supplied through the distributor (primary air) and the secondary air inlets are located at 0.36 m above the distributor. It is equipped with two cyclones. Silica sand and ash were used as bed materials. The weighted average particle sizes in the experimental setup are determined to be 0.56 mm for sand particles. In the experiments, in order to measure the solid particle flux and the gas concentrations, an isokinetic solid particle sampling system and a multi channel gas sampling systems are used [33,58]. The parameters and computation conditions are given in Table 2, including data of Topal [33] which are used to validate the simulation. The design fuel for the bed is a low-grade coal and the composition of coal is shown in Table 3. In the experiments, the solid particle flux, the molar ratio of oxygen, nitrogen oxide and sulphur dioxide emissions were measured along the combustor height and averaged combustor temperature were given.

4.1. Model validation

To test and validate the model presented in this paper, the solid particle flux, the molar ratio of oxygen, nitrogen oxide and sulphur dioxide emissions along the combustor height are obtained for the pilot CFB combustor using the same test data as the simulation program input (Figs. 5 and 6). Inputs for the

Table 2
Experimental conditions [33]

Operating parameters	Values
Coal feed rate (range) (kg/h)	6–7.7
Operation velocity (range) (m/s)	3.60–9.23
Bed temperature (°C)	860–900
Excess air	0.2–0.4
Primary to secondary air ratio	2/3
Ca/S molar ratio	0.5–2.5
Bed area (m^2)	0.0122
Size of coal feed (range) (mm)	0.03–0.9
Mean size of sorbent feed (mm)	0.71

Table 3
Ultimate analysis of Tuncbilek lignite (weight basis)

Elements	%	Dry analysis
C	54.85	59.29
H	4.26	4.61
O	10.64	11.50
N	1.94	2.10
S	1.67	1.81
Ash	19.14	20.60
Moisture	7.5	0.0
H_u (kcal/kg)		5278

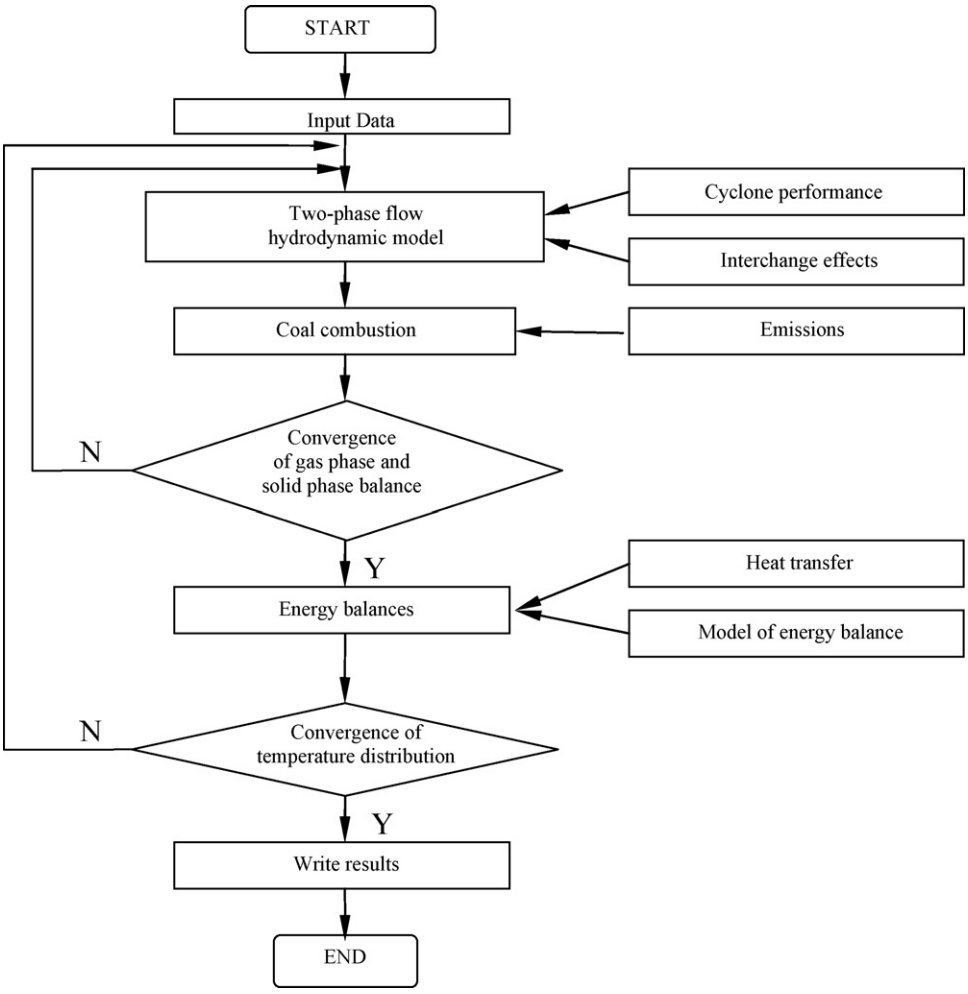

Fig. 3. Flow chart of the numerical solution of the model.

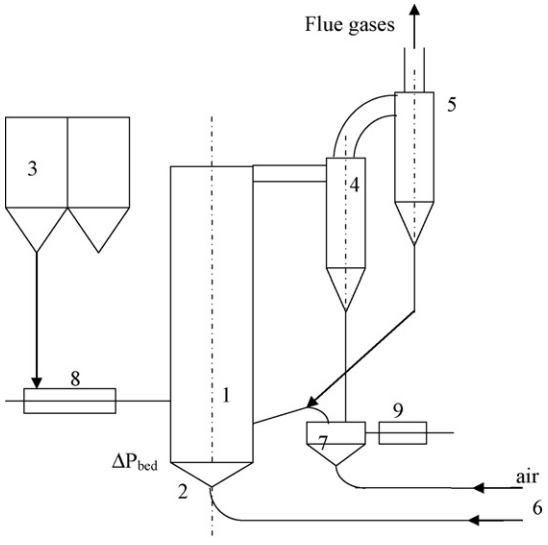

Fig. 4. A schematic diagram of experimental setup: (1) main column (riser); (2) air plenum; (3) fuel bunkers; (4) first cyclone; (5) second cyclone; (6) air blower; (7) re-circulation bed; (8) fuel feeding system; (9) ash handling system [33,58].

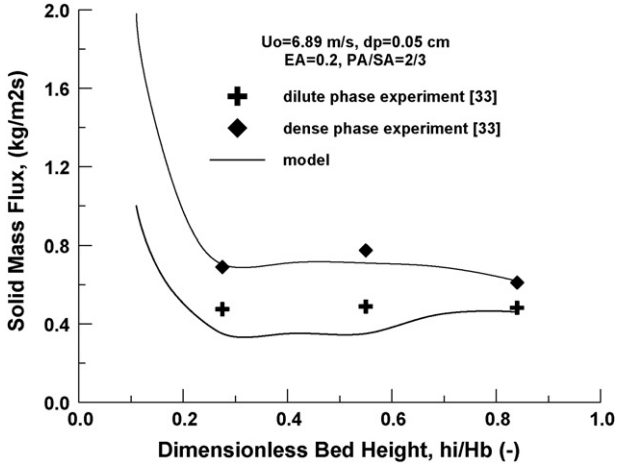

Fig. 5. Variation of solid mass flux along the combustor height. (EA: excess air; PA: primary air; SA: secondary air).

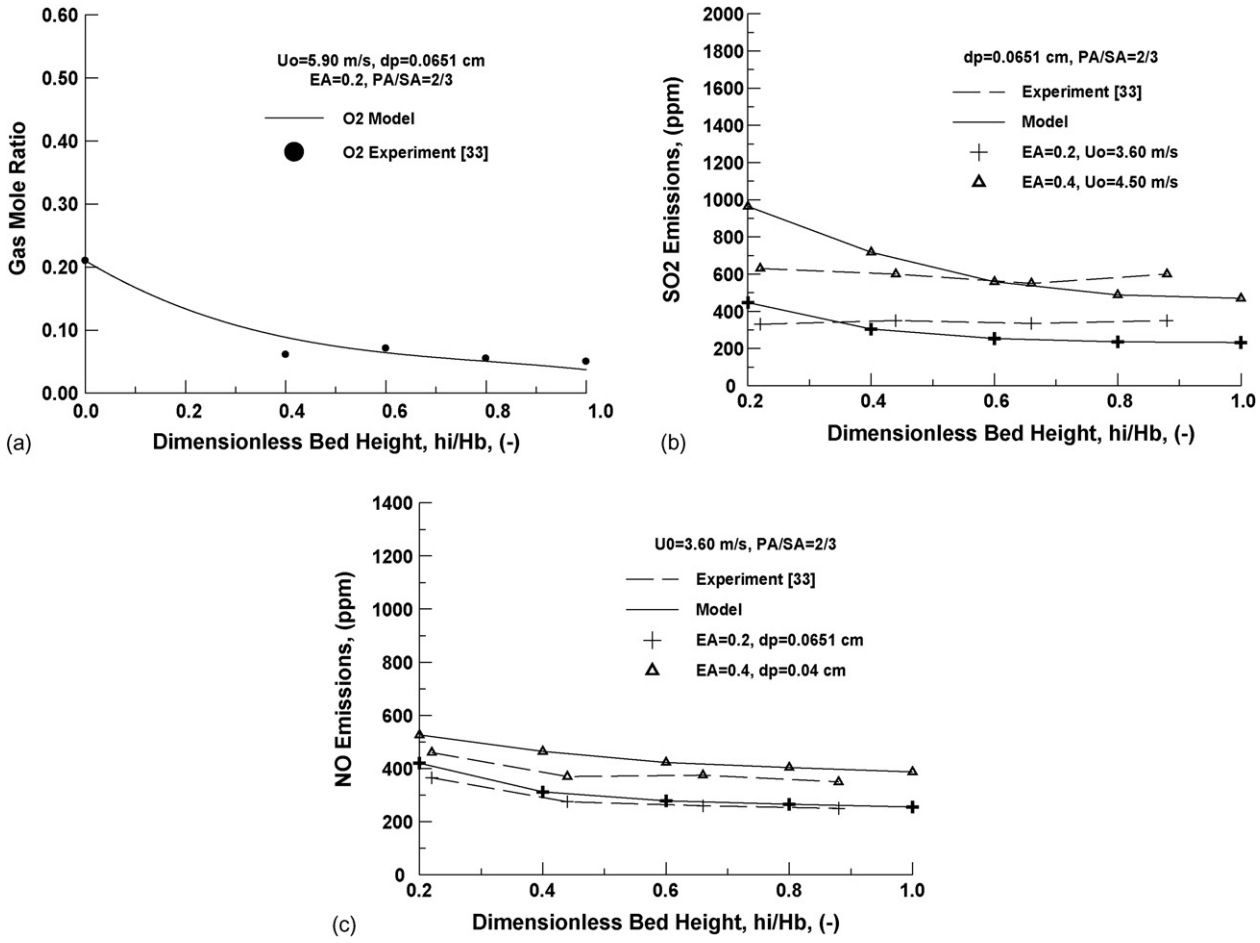

Fig. 6. Comparison of the model and experimental results in respect of O_2, SO_2 and NO concentration changes along the bed height: (a) changes in the O_2 concentration; (b) changes in the SO_2 concentration; (c) changes in the NO concentration.

model are combustor dimensions and construction specifications (insulation thickness and materials, etc.), primary and secondary air flow rates, coal feed rate and particle size, coal properties, Ca/S ratio, limestone particle size, inlet air pressure and temperature, ambient temperature and the superficial velocity. In the model, the cyclone is considered to have 98% collection efficiency.

Fig. 5 shows the predictions and experimental results of the solid particle flux in the dense and dilute phases along the dimensionless combustor height (h_i/H_b). In the experiments, to measure the solid particle flux, an isokinetic solid particle sampling system is used and the solid particle flux in the annulus and core regions is obtained from the measured values as follows:

$$G = \frac{m_{col}}{q} U_0 \tag{19}$$

where m_{col} is the total solid particle holdup, q is the isokinetic gas volume. In the model, the dense phase is characterized by the emulsion phase at the bottom zone and the annulus region at the upper zone. The dilute phase is characterized by the bubble phase at the bottom zone and the core region at the upper zone. The particle flux in the dense phase both in the bottom region and the upper region is higher then the dilute phase. It decreases along the combustor height, but the particle flux in the dense phase increases slightly at the upper part of the riser due to backmixing at the exit and downward flow in the annulus region. Fig. 5 also shows the close agreement between the predicted and experimental results at three measurement points above the secondary air inlet.

The model reasonably predicts oxygen mole ratio along the combustor height in the dense phase as shown in Fig. 6a. Since the experiments are run in a small-scale CFB combustors, there have not been any major differences in O_2 concentrations between the core and the annulus regions at the same bed height in the experimental results [33]. Similar results are observed in the model calculations. Figs. 6b and c present experimental and modeling results for different values of excess air for SO_2 and NO emissions, respectively. According to the model calculations, SO_2 and NO emissions increase with air stagement. That is confirmed by the experimental results. However, the maximum deviation is about 5% for SO_2 and NO emissions at the bed height of 36 cm, the secondary air inlet point. Both the release and combustion of volatiles are influencing factors for the production of NO and SO_2 emissions [15,25,56]. In the model, it is assumed that a great amount of the volatile matters is released at the feed point in the combustor [1,5,8] and sulphur and nitrogen are oxidized to SO_2 and NO immediately. But, because of hydrodynamic behavior of CFB combustor, fast

fluidization in the bottom zone does not allow the volatile to be oxidized to SO_2 and NO. So it leads a minor discrepancy between the model results and experimental data at the bottom zone exit (Figs. 6b and c).

4.2. Effects of operational parameters

Carbon monoxide, carbon dioxide, sulphur dioxide, nitrogen oxides and char content in stack gases are the major pollutants from a CFB combustors with respect to atmospheric environmental conditions. In the present study, the variations of these emissions along the combustor height under different operational conditions such as particle diameter, bed operational velocity and excess air are analyzed with the developed and validated one-dimensional model.

4.2.1. Effects of operational parameters on CO and CO_2 emissions

Model predictions about the effects of operational parameters on CO and CO_2 mole ratios at the dilute and the dense phases are given in Figs. 7 and 8, respectively. During staged combustion, under the secondary air injection point, lack of adequate oxygen presence in the bottom zone, leads to CO formation and carbon monoxide concentration becomes very high along the bottom zone [1,5,6]. Oxygen in the riser increases while carbon monoxide emission sharply decreases and results in an increase of CO_2 mole ratio caused by the secondary air supply at the 0.36 m bed height above the distributor plate as shown in Figs. 7 and 8. In addition to increment of oxygen mole ratio, the sharp decrement in CO emissions after the secondary air point is caused by the combustion rate of char depending on the bed temperature and coal particle diameter where the ratio of primary to secondary air is taken into account as 2/3 in the model (Figs. 7a and 8a).

The discrepancy between the CO mole ratio values in the dense phase and the dilute phase is due to the higher char particle concentration and the lower oxygen presence in the dense phase in comparison to the dilute phase in Figs. 7 and 8.

Because very rare char particles exist in the dilute phase main source of the CO_2 concentration is due to the oxidation of the CO since an adequate amount of oxygen exist in this phase. This causes a continuously increasing trend in CO_2 emission values (Fig. 7a). At the same time due to higher numbers of char particle presence in dense phase; CO and CO_2 concentrations depend on both combustion of coal and CO reduction oxidation [1]. This situation results in higher CO_2 concentrations with respect to dilute phase (Fig. 8a).

As the operational velocity increases particle residence time in the combustor, char combustion rate and bed temperature decrease which results in higher CO emission values in both dilute and dense phases (Figs. 7b and 8b). With the increase of temperature, the reaction rate constant of char combustion increases, which leads to lower char and CO concentration in the

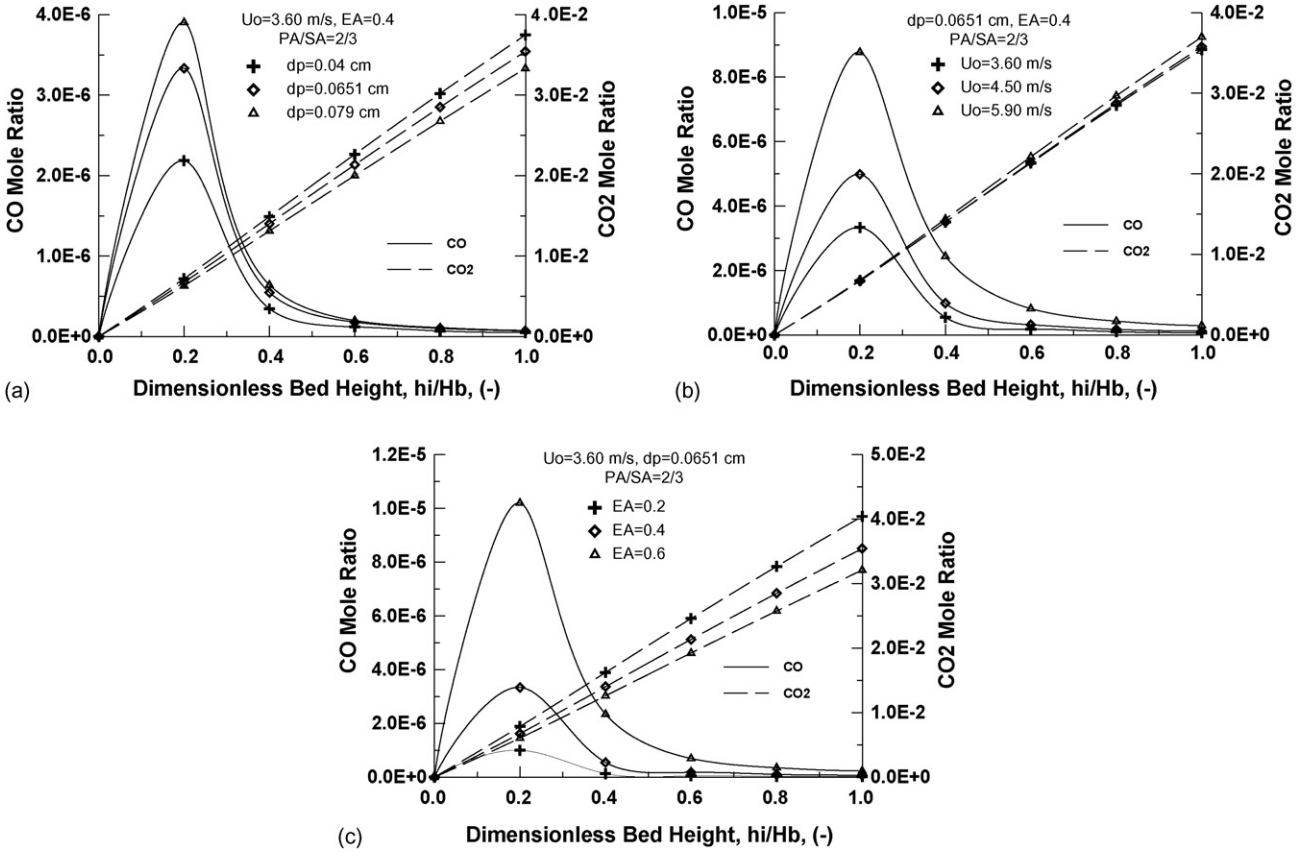

Fig. 7. Effects of operational parameters on CO and CO_2 mole ratios at dilute phase along the bed height: (a) effect of coal particle size; (b) effect of superficial velocity; (c) effect of excess air.

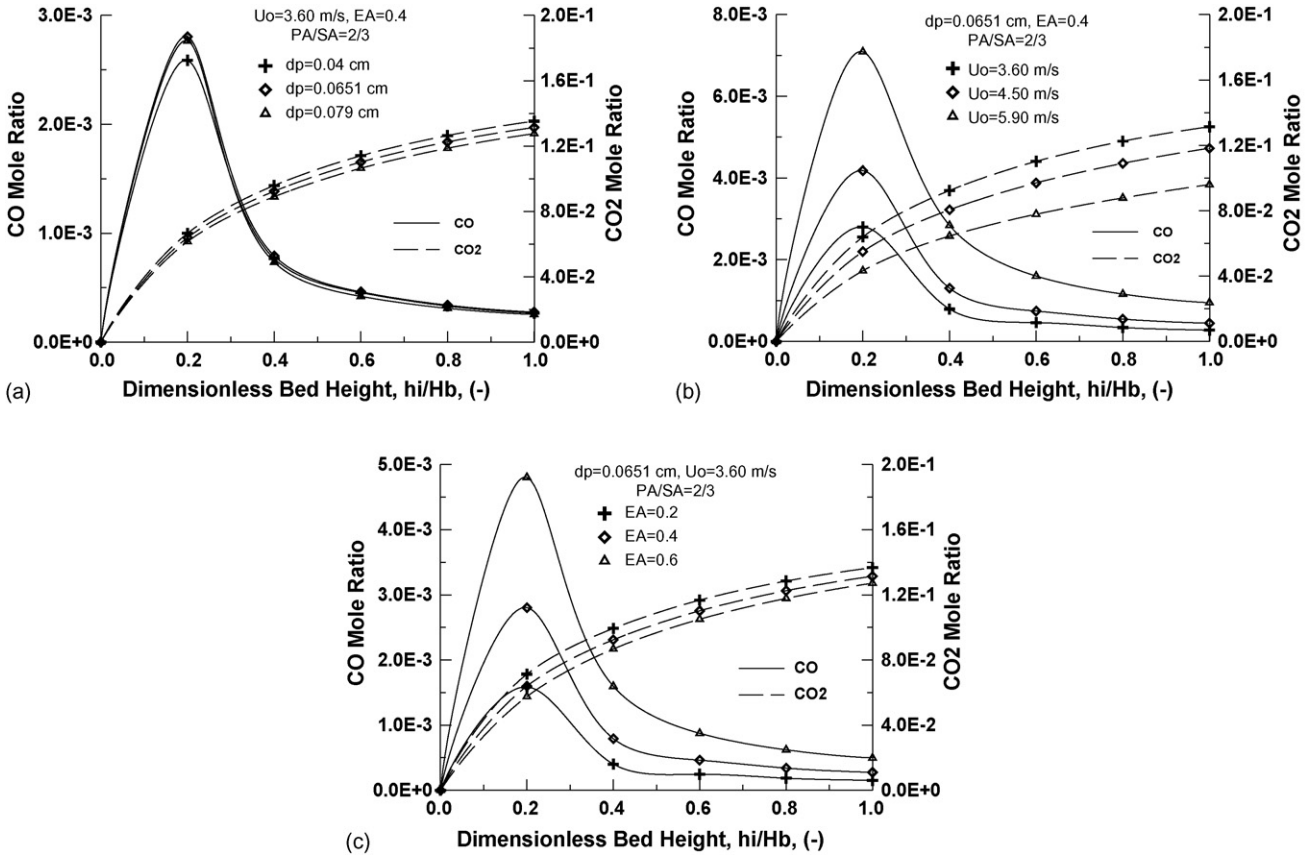

Fig. 8. Effects of operational parameters on CO and CO_2 mole ratios at dense phase along the bed height: (a) effect of coal particle size; (b) effect of superficial velocity; (c) effect of excess air.

combustor (Figs.7b and Fig. 8b). When compared to the dilute phase, it is clearly seen from Fig. 8b, the bed operational velocity plays an important role on CO_2 emissions in dense phase due to decrease in particle residence time and lower combustion rates.

Figs. 7c and 8c present simulation results for different values of the excess air. With the increase of excess air level the bed temperature decreases and generates a decrease of the CO oxidation rate constant. As it is seen from the figures, CO emissions noticeably increase when excess air increases in the bottom zone whereas the concentration of CO_2 decreases as the excess air increases along the bed height. This phenomenon is also observed in the studies of Ducarne et al. [57]. Another explanation of decreasing CO_2 emissions is the gas dilution caused by increasing excess air. As it is observed from Figs. 7 and 8, CO emissions sharply decrease while CO_2 emissions increase with air stagement at the dilute and the dense phases. As a result of model predictions presented, CO and CO_2 emissions have been affected significantly by bed operational velocity in the dense phase and by excess air in the dilute phase.

4.2.2. *Effects of operational parameters on NO emissions*

Nitrogen oxides are a major environmental pollutant resulting from combustion. The reactions of nitric oxide with carbons or chars are of current interest with regard to their possible role in reducing NO emissions from combustion systems. They also offer new useful insights into the oxidation reactions of carbons, generally [13]. In the model, char reduces NO to N_2 according to the reaction given in Table 1.

The emission of NO depends on temperature because the NO oxidation changes significantly with temperatures [19]. It must also be noted that together with this, at the operating temperature of the CFB combustor (between the temperatures 800 and 950 °C), nitrogen in air does not take part in an oxidation reaction to form NO.

Model predictions about the effects of operational parameters on NO emissions at the dilute and the dense phases are given in Fig. 9. The mass transfer between the dilute and the dense phase due to the NO concentration differences causes a continuous increase in NO emissions in the dilute phase. The reduction of NO to N_2 by char particles in the model leads to a lower concentration of NO in the dilute phase when compared to the dense phase caused by lack of enough char particles. The results of Lin et al.'s [59] study verify this phenomenon. Moreover the results of Kilpinen et al.'s [19] study show that during char particle combustion, the net conversion of char-N to NO increases strongly when temperature is increased from 773 to 1073 K and at temperatures 1073–1273 K a plateau is reached. Fig. 11 clearly indicates that after dimensionless bed height of 0.6, the bed temperature is within the range of 1073–1273 K and from that point on NO emission profiles form a plateau in dense phase (Fig. 9).

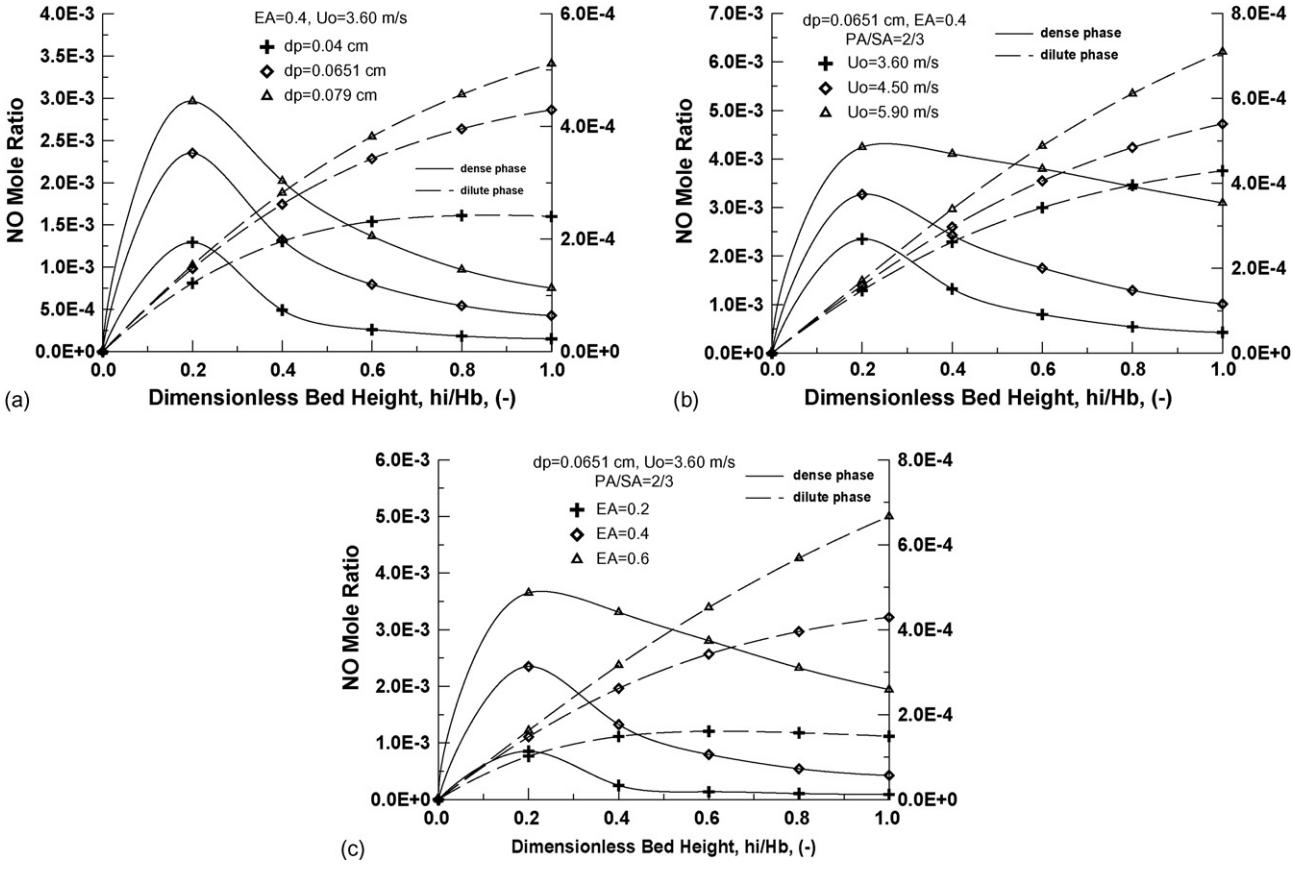

Fig. 9. Effects of operational parameters on NO mole ratio at dilute and dense phase along the bed height: (a) effect of coal particle size; (b) effect of superficial velocity; (c) effect of excess air.

In the dense phase, due to high char concentration especially at the bottom zone fuel related NO formation is higher than the dilute phase. A smaller mean size of char in the combustor will result in a lower emission of NO if other parameters are kept unchanged [25] as clearly seen from Fig. 9a.

Fig. 9b illustrates the effect of bed operating velocity on NO emissions. The bed operational velocity in the combustor is one of the basic design variables of the process. The reason is that with the increase of bed operating velocity the hydrodynamic condition of the combustor changes. Suspension density in the bottom zone decreases with the increase of superficial velocity. So, the contact time of NO with char particles decreases, thus reducing the rate of reduction of NO. Therefore, NO emissions increase with increasing superficial velocity.

Oxygen concentration plays a major role in NO related reactions. Fig. 9c shows that higher excess air level gives higher emission levels of NO, because formation of NO increases with the increase of oxygen concentration. At the bottom zone NO concentration is higher when the excess air increases, although there is more dilution. This can be explained by a strong O_2 concentration that induces NO formation from volatiles, but also by a faster combustion which liberates the fixed nitrogen as NO. With the increase of excess air level the combustion rate of char increases which results in the reduction of char content in the combustor, thus, the reduction rate of NO decreases. These results are verified by the experimental results from the literature [9,24,52,54].

4.2.3. *Effects of operational parameters on SO_2 emissions*

Model predictions about the influence of the bed operational parameters on SO_2 emissions are shown in Fig. 10 which plots the variation of the SO_2 emissions along bed height for three different particle diameters, bed operational velocities and excess air values.

In CFB combustor, the SO_2 generation and retention processes take place simultaneously in the bed. As mentioned above, the SO_2 generation rate from the char depends on its combustion rate, which depends on the temperature, excess air, O_2 concentration, etc. [59].

Fig. 10a illustrates the effect of particle diameter on SO_2 emissions. Increase of the size of particle increases the SO_2 concentration in both phases. The SO_2 emission values with particle diameter of 0.04 cm, which had a higher proportion of fine particles, were lower than those obtained with particle diameter of 0.0651 cm and of 0.079 cm. This was due to the effect of the particle size distribution on solids circulation flow rate, which increases when the mean particle size in the bed decreases. Thus, the mean residence time of the fine sorbent particles in the bed decreases and they are not completely recovered by the cyclone.

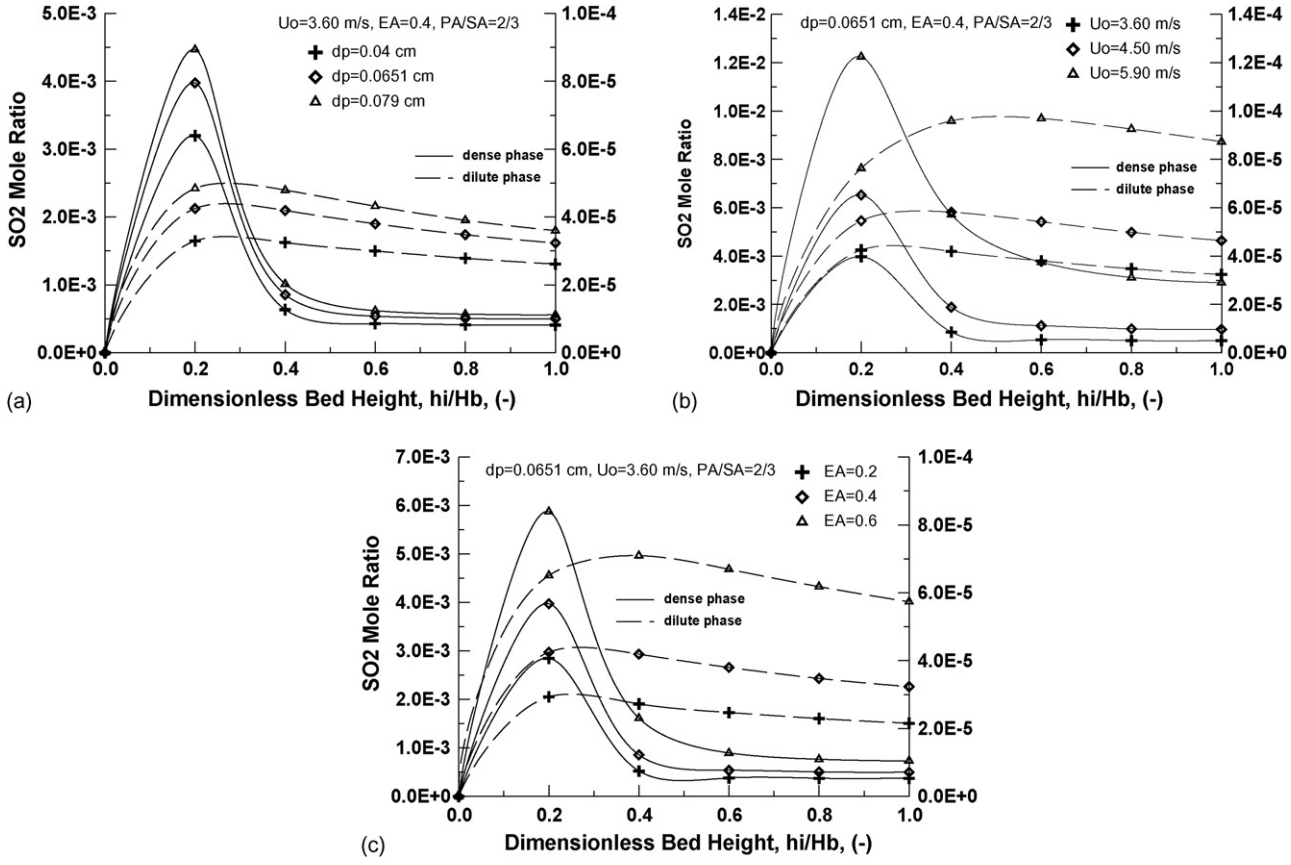

Fig. 10. Effects of operational parameters on SO_2 mole ratio at dilute and dense phase along the bed height: (a) effect of coal particle size; (b) effect of superficial velocity; (c) effect of excess air.

To analyze the effect of the bed operational velocity on SO_2 emission along the bed height, particle diameter 0.0651 cm is used with three different bed operational velocity values. An increase in air velocity decreases sulphur retention since it increases the flow rates of circulating solids, and thus decreases the mean residence time of limestone particles and their conversion in the bed (Fig. 10b).

Fig. 10c plots the predicted SO_2 emissions as a function of the dimensionless bed height at particle diameter 0.0651 cm, at bed operational velocity 3.60 m/s with excess air values 0.2, 0.4 and 0.6. The efficiency of desulphurization decreases as the excess air ratio increases [59]. Figure shows that a higher excess air level gives higher emission levels of SO_2 because formation of SO_2 increases with the increase of oxygen concentration. At the bottom zone, increase of excess air leads to higher concentrations of O_2 and this result causes SO_2 formation from volatiles, but also by a faster combustion which liberates the fixed sulphur as SO_2. The results shown in Fig. 10c are also verified by the experimental study of Adanez et al. [60].

4.2.4. Effects of operational parameters on char content in stack gases

The char content in stack gases is one of the major emission pollutants in atmospheric environmental conditions. Using the solid separator and having the efficient combustion conditions, the char content in stack gases is reduced to minimum levels in CFB combustors. In this study, the variations of this emission along the combustor height under different operational conditions such as particle diameter, bed operational velocity and excess air are analyzed through the developed model (Fig. 11).

The temperature decrease generates a combustion efficiency decrease, and thus higher carbon content in the combustor which is clearly seen in Fig. 11. With the increase of temperature, the reaction rate constant of char combustion increases, which leads to lower char concentration in the combustor and lower CO concentration (Fig. 7b and Fig. 11).

The carbon content depends on temperature and the combustion rate of char which could be determined from the kinetic model of char combustion. As the particle diameter increases, char combustion rate and in consequence bed temperature decreases and this situation causes higher char concentration in the combustor (Fig. 11a). The superficial velocity affects the mean residence time of the char particle. Residence time decreases the combustion efficiency of char and therefore gives higher carbon content as shown in Fig. 11b.

As shown in Fig. 11c, higher excess air levels result in lower carbon content, because the combustion rate of char increases by amount of oxygen presence which is also verified by the experimental study of Lin et al. [59].

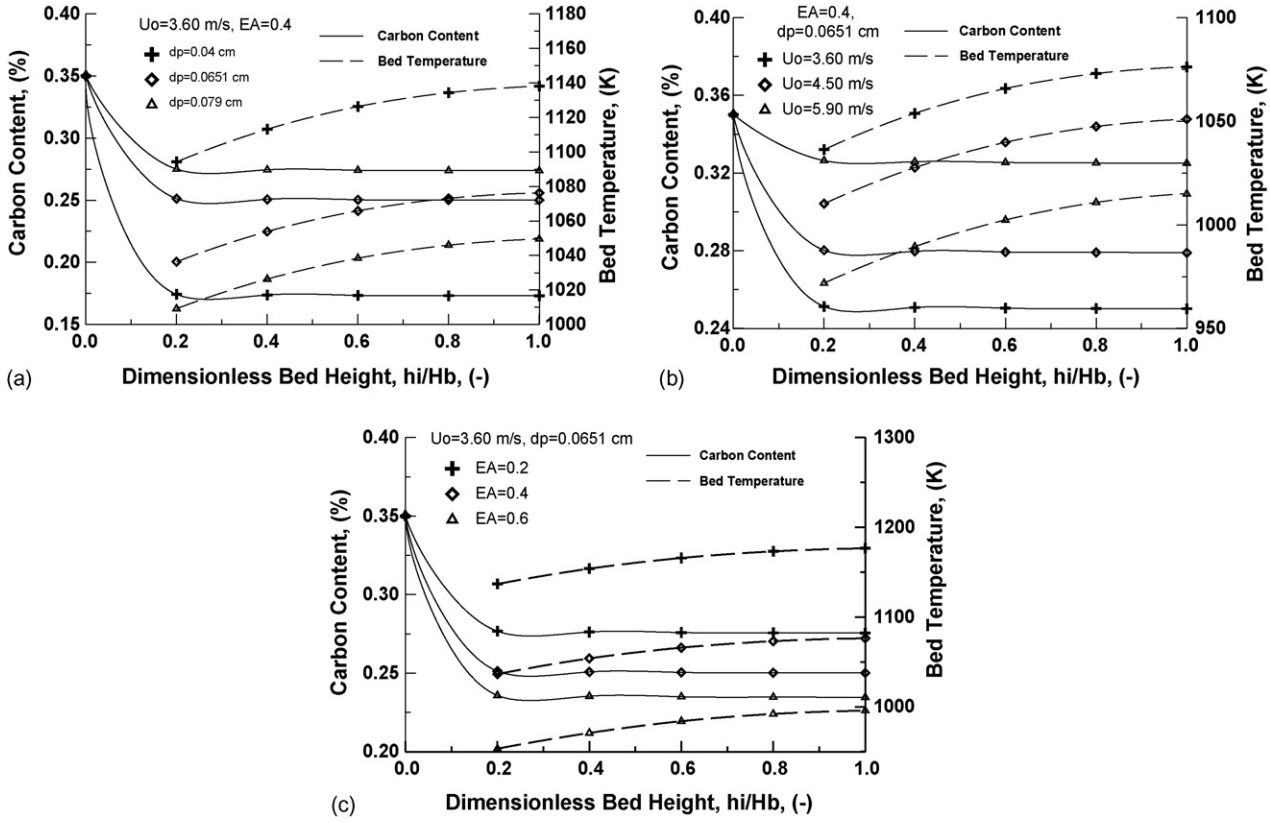

Fig. 11. Effects of operational parameters on carbon content and bed temperature along the bed height: (a) effect of coal particle size; (b) effect of superficial velocity; (c) effect of excess air.

5. Conclusions

In this study, a 1D model for a CFB combustor has been developed which integrates and simultaneously predicts the hydrodynamics and combustion aspects. The model has been validated against the data from the literature [33]. Using the developed model, effects of operational parameters such as particle diameter, superficial velocity and excess air on carbon monoxide, carbon dioxide, sulphur dioxide, nitrogen oxides emissions and char content along the combustor height are investigated:

- CO and CO_2 emissions have been affected significantly by bed operational velocity in the dense phase and by excess air in the dilute phase.
- A smaller mean size of char in the combustor result in a lower emission of NO if other parameters is kept unchanged. NO emissions increase with the superficial velocity of the combustor. The higher excess air levels give higher emission levels of NO.
- Increase of the size of particle increases the SO_2 concentration. An increase in superficial velocity decreases sulphur retention. The higher excess air level gives higher emission levels of SO_2.
- As the particle diameter increases, char combustion efficiency and in consequence bed temperature decreases and results in higher char concentration. The increasing superficial velocity decreases the combustion efficiency of char and therefore gives higher carbon content. The higher excess air levels result in lower carbon content.

The present study proves that CFB combustion allows clean and efficient combustion of coal which is demonstrated by the fact that both experimental data and model simulation results have low and acceptable level of emission pollutants.

References

[1] P. Basu, Combustion of coal in circulating fluidized-bed boilers: a review, Chem. Eng. Sci. 54 (1999) 5547–5557.
[2] P. Basu, A. Sett, E.A.M. Gbordzoe, A simplified model for combustion of carbon in a circulating fluidized bed combustor, in: J.P. Mustonen (Ed.), Proceedings of the IX International Conference on Fluidized Bed Combustion, ASME, New York, 1987, pp. 738–742.
[3] I. Heinbockel, F.N. Fett, Simulation of a combined cycle power based on a pressurized circulating fluidized bed combustor, in: P. Basu (Ed.), Heat Recovery System & CHP, N. 2, vol. 15, Pergamon Press, Oxford, 1995, pp. 171–178.
[4] C.G. Remberg, A. Nemet, F.N. Fett, Towards a more general process model for power plants with atmospheric or pressurized fluidized bed combustion, in: F.D.S. Preto (Ed.), Proceedings of the 14th International Conference on Fluidized Bed Combustion, vol. 2, ASME, sNew York, 1997, pp. 1139–1149.
[5] L. Huilin, Z. Guangbo, B. Rushan, C. Yongjin, D. Gidaspow, A coal combustion model for circulating fluidized bed boilers, Fuel 79 (2000) 165–172.
[6] J. Adanez, P. Gayan, L.F. Diego, L. Armesto, A. Cabanillas, Circulating fluidized bed combustion in the turbulent regime: modeling of

carbon combustion efficiency and sulfur retention, Fuel 80 (2001) 1405–1414.
[7] Q. Wang, Z. Luo, M. Ni, K. Cen, Particle population balance model for a circulating fluidized bed boiler, Chem. Eng. J. 93 (2003) 121–133.
[8] Y. Hua, G. Flamant, J. Lu, D. Gauthier, Modelling of axial and radial solid segregation in a CFB boiler, Chem. Eng. Process. 43 (8) (2003) 971–978.
[9] Y.H. Zhou, H.L. Lu, Y.R. He, Numerical prediction of combustion of carbon particle clusters in a circulating fluidized bed riser, Chem. Eng. J. 118 (1/2) (2006) 1–10.
[10] T. Knoebig, K. Luecke, J. Werther, Mixing and reaction in the circulating fluidized bed—a three-dimensional combustor model, Chem. Eng. Sci. 54 (1999) 2151–2160.
[11] T. Hyppanen, Y.Y. Lee, A. Rainio, A three-dimensional model for circulating fluidized bed combustion, in: P. Basu, M. Horio, M. Hasatani (Eds.), Circulating Fluidized Bed Technology III, Pergamon Press, Oxford, 1991, pp. 563–568.
[12] Y.P. Tsuo, Y.Y. Lee, A. Rainio, T. Hyppanen, Study of $SO_2/NO_2/N_2O$ emission from CFB boilers with a three-dimensional CFB combustion model, in: M. Kwauk, J. Li (Eds.), Circulating Fluidized Bed Technology V, Science Press, Beijing, 1997, pp. 466–481.
[13] I. Aarna, E.M. Suuberg, The role of carbon monoxide in the NO-carbon reaction, Energy Fuels 13 (1999) 1145–1153.
[14] I. Aarna, E.M. Suuberg, A review of the kinetics of the nitric oxide-carbon reaction, Fuel 76 (1997) 475–482.
[15] Y.H. Li, G.Q. Lu, V. Rudolph, The kinetics of NO and N_2O reduction over coal chars in fluidized bed combustion, Chem. Eng. Sci. 53 (1998) 1–7.
[16] H. Aoki, A. Suzuki, Y. Hisaeda, Y. Suwa, T. Nakagawa, M. Yaga, M. Shoji, T. Miura, Recent research and development of combustion simulation, Heat Transfer Asian Res. 30 (7) (2001) 581–612.
[17] I.M. Bews, A.N. Hayhurst, S.M. Richardson, S.G. Taylor, The order, Arrhenius parameters, and mechanism of the reaction between gaseous oxygen and solid carbon, Combust. Flame 124 (2001) 231–245.
[18] R. Abe, H. Sasatsu, T. Harada, N. Misawa, I. Saitou, Prediction of emission gas concentration from pressurized fluidized bed combustion (PFBC) of coal under dynamic operation conditions, Fuel 80 (2001) 135–144.
[19] P. Kilpinen, S. Kallio, J. Konttinen, V. Barisic, Char-nitrogen oxidation under fluidised bed combustion conditions: single particle studies, Fuel 81 (2002) 2349–2362.
[20] H. Liu, B. Feng, J.D. Lu, Coal property effects on N_2O and NO_x formation from circulating fluidized bed combustion of coal, Chem. Eng. Commun. 192 (10–12) (2005) 1482–1489.
[21] Y. Zhao, P.Y. Xu, D. Fu, Experimental study on simultaneous desulfurization and denitrification based on highly active absorbent, J. Environ. Sci. China 18 (2) (2006) 281–286.
[22] F. Winter, Single Fuel Particle and NO_x/N_2O-Emission Characteristics Under Circulating Fluidized Bed Combustor Conditions, Ph.D. Thesis, University of Technology, Vienna, Austria, 1995.
[23] M. Stenseng, W. Lin, J.E. Johnsson, K.D. Johansen, Modeling of devolatilization in CFB combustion, in: F.D.S. Preto (Ed.), Proceedings of the 14th International Conference on Fluidized Bed Combustion, vol. 1, ASME, New York, 1997, pp. 117–124.
[24] P. Kilpinen, P. Glarborg, M. Hupa, Reburning chemistry at fluidized bed combustion conditions-a kinetic modeling study, Ind. Eng. Chem. Res. 31 (1992) 1477–1490.
[25] J. Talukdar, P. Basu, A simplified model of nitric oxide emission from a circulating fluidized bed combustor, Can. J. Chem. Eng. 73 (1995) 635–643.
[26] S. Goel, A. Sarofim, P. Kilpinen, M. Hupa, Emissions of nitrogen oxides from circulating fluidized bed combustors: modeling results using detailed chemistry, in: Proceedings of the 26th International Symposium on Combustion, The Combustion Institute, Naples, 1996.
[27] D. Barletta, A. Marzocchella, P. Salatino, Modelling the SO_2–limestone reaction under periodically changing oxidizing/reducing conditions: the influence of cycle time on reaction rate, Chem. Eng. Sci. 57 (2002) 631–641.
[28] M.J. Fernandez, H. Kasman, A. Lyngfelt, Methods for measuring the concentrations of SO_2 and gaseous reduced sulphur compouds in the combustion chamber of a circulating fluidized bed boiler, Can. J. Chem. Eng. 78 (2000) 1138–1144.
[29] A. Svensson, F. Johnsson, B. Leckner, Fluid-dynamics of the bottom bed of circulating fluidized bed boilers, in: Proceedings of XII International Conference on Fluidized Bed Combustion, San Diego, CA, 1993, pp. 887–897.
[30] J. Werther, J. Wein, Expansion behavior of gas fluidized beds in the turbulent regime, AIChE Symp. Ser. 301 (90) (1994) 31–44.
[31] B. Leckner, M.R. Golriz, W. Zhang, B.A. Andersson, F. Johnsson, Boundary layers first measurement in the 12 MW CFB plant at Chalmers University, in: Eleventh International Conference on Fluidized Bed Combustion, ASME, 1991, pp. 771–776.
[32] D. Montat, T.D. Maggio, 1D two-phase description of the thermal hydraulic behavior of the furnace of E. Huchet 125 MWe CFB boiler, in: Fifth International Conference on CFB, MSR6, Beijing, 1996.
[33] H. Topal, Experimental Investigation of the Hydrodynamic, Combustion and Emission Properties of a Circulating Fluidized Bed, Ph.D. Thesis, Gazi University Institute of Science and Technology, The Turkey, Gazi University Press, 1999.
[34] N. Eskin, A. Gungor, A model for circulating fluidized bed combustors, in: Proceedings of the First International Exergy, Energy and Environment Symposium, 2003, pp. 911–918.
[35] M.J. Rhodes, D. Geldart, The upward flow of gas/solid suspensions, Part 2. A practical quantitive flow regime diagram for the upward flow of gas/solid suspensions, Chem. Eng. Res. Des. 67 (1989) 30–37.
[36] L. Huilin, B. Ruhsan, Y. Lidan, Z. Guangbo, T. Xiu, Numerical computation of a circulating fluidized bed combustor, Int. J. Energy Res. 22 (1998) 1351–1364.
[37] N. Eskin, A. Kılıç, Calculation of steady-state operation characteristics of fluidized bed coal combustors, Bull. Istanbul Tech. Univ. 48 (1995) 11–36.
[38] N. Eskin, A. Gungor, Hydrodynamic simulation of circulating fluidized bed, in: Proceedings of 9th International Research/Expert Conference on Trends in the Development of Machinery and Associated Technology, TMT 2005, Antalya, Turkey, 2005, pp. 673–676.
[39] R.R. Rajan, C.Y. Wen, A comprehensive model for fluidized bed coal combustors, AIChE J. 26 (1980) 642–655.
[40] S. Mori, C.Y. Wen, Estimation of bubble diameter in gaseous fluidized beds, AIChE J. 21 (1975) 109–117.
[41] C.Y. Wen, Y.H. Yu, Mechanics of fluidization, Chem. Eng. Prog. Symp. Ser. 62 (1966) 100–110.
[42] Q. Wang, Z. Luo, X. Li, M. Fang, M. Ni, K. Cen, A mathematical model for a circulating fluidized bed (CFB) boiler, Energy 24 (1999) 633–653.
[43] Y.C. Ray, T.S. Jiang, Particle population model for a fluidized bed attrition, Powder Technol. 52 (1987) 35.
[44] R. Chirone, L. Massimilla, P. Salatino, Communication of carbon in fluidized bed combustion, Prog. Energy Combust. Sci. 17 (1991) 297.
[45] U. Arena, A. Cammarota, L. Massimilla, L. Siciliano, P. Basu, Carbon attrition during the combustion of a char in a circulating fluidized bed, Combust. Sci. Technol. 73 (1990) 383–392.
[46] C.A. Palmer, E. Tuncali, K.O. Dennen, T.C. Coburn, R.B. Finkelman, Characterization of Turkish coals: a nationwide perspective, Int. J. Coal Geol. 60 (2–4) (2004) 85–115.
[47] D. Shi, R. Nicolai, L. Reh, Wall-to-bed heat transfer in circulating fluidized beds, Chem. Eng. Process. 37 (1998) 287–293.
[48] C. Brereton, Combustion performance, in: A. Avidan, J.R. Grace, T. Knowlton (Eds.), Circulating Fluidized Beds, Blackie Academic & Professional, London, 1997, p. 388.
[49] P.K. Agarwal, A single particle model for the evolution and combustion of coal volatiles, Fuel 65 (1986) 803–810.
[50] D.R. Gregory, R.F. Littlejohn, A survey of numerical data on the thermal decomposition of coal, BCURA Monthly Bull. 29 (6) (1965) 173–179.
[51] R. Loison, R. Chauvin, Pyrolyse rapide du charbon, Chem. Ind. 91 (1964) 269–274.
[52] D.H. Fine, S.M. Slater, A.F. Sarofim, G.C. Williams, Nitrogen in coal as a source of nitrogen oxide emission from furnaces, Fuel 53 (1974) 120–128.
[53] M.A. Field, D.W. Gill, B.B. Morgan, P.W.G. Hawksley, Combustion of pulverized coal, Coal Util. Res. Assoc. 31 (6) (1967) 285–292.
[54] H.C. Hottel, G.C. Williams, N.M. Nerheim, G.R. Schneider, Burning rate of carbon monoxide, in: Proceedings of the 10th International Sympo-

sium on Combustion, The Combustion Institute, Pittsburgh, 1965, pp. 111–117.
[55] R.H. Borgwardt, Kinetics of the reaction of SO_2 with calcined limestone, Environ. Sci. Technol. 4 (1970) 49–57.
[56] S.E. Tung, G.C. Williams, Atmospheric Fluidized Bed Combustion, Massachusetts Institute of Technology, Cambridge, MA, 1987.
[57] E.D. Ducarne, J.C. Dolignier, E. Marty, G. Martin, L. Delfosse, Modelling of gaseous pollutants emissions in circulating fluidized bed combustion of municipal refuse, Fuel 77 (1998) 1399–1410.
[58] H. Topal, A.T. Atimtay, A. Durmaz, Olive cake combustion in a circulating fluidized bed, Fuel 82 (2003) 1049–1056.
[59] C.H. Lin, J.T. Teng, C.S. Chyang, Evaluation of the combustion efficiency and emission of pollutants by coal particles in a vortexing fluidized bed, Combust. Flame 110 (1997) 163–172.
[60] J. Adanez, L.F. de Diego, P. Gayan, L. Armesto, A. Cabanillas, Modeling of sulfur retention in circulating fluidized bed combustors, Fuel 75 (3) (1996) 262–270.